Available online at www.sciencedirect.com
ScienceDirect
Journal of Molecular Catalysis A: Chemical 263 (2007) 163–168
JOURNAL OF MOLECULAR CATALYSIS A: CHEMICAL
www.elsevier.com/locate/molcata

Recyclable nano-size Pd catalyst generated in the multilayer polyelectrolyte films on the magnetic nanoparticle core

Yuhong Wang [a], Jin-Kyu Lee [b,*]

[a] *Department of Chemical Engineering, Shanghai Institute of Technology, Shanghai 200235, PR China*
[b] *School of Chemistry, College of Natural Science, Seoul National University, Seoul 151-747, South Korea*

Received 8 March 2006; received in revised form 18 August 2006; accepted 21 August 2006
Available online 26 August 2006

Abstract

This work describes the preparation of Pd nanoparticles in multilayer polyelectrolyte films fabricated on a magnetic ferrite core by a layer-by-layer (LbL) self-assembly technique, and the relationship between catalytic activity and these hybrid core-shell nanocomposite structures in the hydrogenation of olefinic alcohols. The hydrogenation reaction seems to be only catalyzed by Pd nanoparticles in the outermost layer of the hybrid composites, probably due to the restricted diffusion of olefinic alcohols into ionically cross-linked multilayer films. The nano-size Pd catalysts attached to the core magnetic nanoparticles (MNP, $CoFe_2O_4$; average size = 20 nm) could be easily and efficiently isolated from the final product solution by magnetic decantation (applying external magnetic field), and be reused for 10 consecutive reactions without showing any significant activity degradation.

Keywords: Recyclable catalyst; Nano-catalyst; Polyelectrolyte; LbL multilayer film

1. Introduction

Intensive studies on a particle size effect of expensive transition metal catalysts such as Pd have been carried out in conventional catalyst systems for commercial applications [1–5], and various synthetic methods and catalytic efficiencies of Pd in nanometer sizes have also been investigated [6–8]. It has been well recognized that the reaction rate per unit catalyst surface area can vary with particle size, and decreasing particle size will not always result in an increased reaction rate per unit mass of transition metal [9–12]. Controlling the size of naked Pd nanoparticles is not easy to achieve because they tend to aggregate. In order to solve this problem, many ideas have been suggested such as immobilizing Pd nanoparticles on solid supports (carbon, Al_2O_3, SiO_2 and MCM-41) [13–18] and modifying the surface of Pd nanoparticle with stabilizers such as surfactants or polymers [19–23]. The surface of nanoparticles was also modified by layer-by-layer (LbL) self-assembled multilayer films, and this method proved to have many advantages such as diversity of film composition and controllability of the thickness of the polymer films [24–27].

In our work, the fabrication of Pd nanoparticle catalysts supported on magnetic nanoparticles (MNPs) starts from the LbL self-assembled multilayer films of poly(acrylic acid) (PAA) and a polyethylenimine–Pd(II) complex (PEI–Pd(II)) on the surface of magnetic nanoparticles (MNPs) by a modification of the known method [28]. The subsequent reduction of Pd(II) by $NaBH_4$ yields catalytic Pd(0) nanoparticles embedded in LbL multilayer films of $[PEI–Pd(II)/PAA]_n$ (Scheme 1). From the catalytic activity of these hybrid core-shell nanocomposites having different Pd structures in the hydrogenation of olefinic alcohols, it was concluded that Pd nanoparticles only in the outermost layer of the hybrid composites could work as a catalyst. Owing to the magnetic property from the core MNP of the present homogeneously dispersed nanocomposite system, furthermore, it could be conveniently separated and controlled by an external magnetic field for recycling.

2. Experimental

2.1. Materials

Polyethylenimine (PEI) ($M_w = 25\ 000$), poly(acrylicacid) (PAA) (35 wt% in water, $M_w = 8000$), allyl alcohol (99%), 3-buten-2-ol (99%), 1-penten-3-ol (99%), potassium tetra-

* Corresponding author. Tel.: +82 2 879 2923; fax: +82 2 882 1080.
E-mail address: jinklee@snu.ac.kr (J.-K. Lee).

1381-1169/$ – see front matter © 2006 Elsevier B.V. All rights reserved.
doi:10.1016/j.molcata.2006.08.069

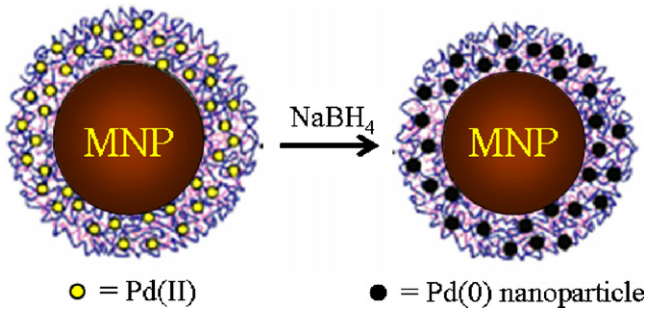

Scheme 1. Formation of Pd nanoparticles in MPFs supported by MNPs.

chloropalladate(II) (99%) and sodium borohydride were purchased from Aldrich. All reagents were used as received, and solutions were prepared with deionized water. Bare Co-ferrite nanoparticles (MNPs) were prepared by the co-precipitation method [29].

2.2. Preparation of nanocomposite catalysts MNP@PAA[PEI–Pd(0)/PAA]$_n$

One milliliter of bare MNP solution (0.3 mg/mL, positive charge) was mixed with 0.4 mL of PAA solution (10 mg/mL, the pH adjusted to 6.5, negative charge), and stirred vigorously for 30 min. Subsequently, the solution was ultracentrifuged, and the supernatant solution was decanted. The PAA-coated MNPs were then washed with 5 mL of deionized water to remove the excess PAA by ultracentrifugation. After that the PAA-coated MNPs were dispersed into 1 mL deionized water again. To deposit a polycation layer, 0.4 mL of a PEI (or PEI–Pd(II)) solution (10 mg/mL PEI, 20 mM K_2PdCl_4, pH adjusted to 7.5) was added to the PAA-coated MNPs solution, and the solution was stirred and washed as described above. The procedures were repeated until the desired number of bilayers of PAA/PEI (or PAA/PEI–Pd(II)) were deposited. Reduction of the Pd(II) in the films was carried out by treating 1 mL PAA/PEI–Pd(II)-coated MNPs solution with 2 mL of fresh 1.0 mM $NaBH_4$ solution for 30 min to provide PAA/PEI–Pd(0)-coated MNPs. The particles were washed three times with water after exposure to $NaBH_4$. MNP@PAA[PEI–Pd(0)/PAA]$_n$ catalysts easily dispersed upon exposure to aqueous hydrogenation solutions.

2.3. Characterization of catalysts MNP@PAA[PEI–Pd(0)/PAA]$_n$

TEM was performed on a JEOL JEM-3000F microscope using an accelerating voltage of 80 kV. ICP-MS data were recorded from VG Elemental/PQ2-Turbo. Sample solutions were prepared by dissolving 0.5 mL catalyst in 0.5 mL of *aqua regia* for 15 min. Then these sample solutions were diluted to 10 mL with deionized water and analyzed. XPS (X-ray photoelectron spectroscopy) measurements were performed on coated silica wafers using Ariesarse 10MCD 150 workshop (UK). The thicknesses of samples were determined by the times of dipping sample solutions on silica wafers.

UV–visible absorption spectra were measured in a quartz cell using a Hitachi U-2300 UV–visible spectrometer. Four milliliters of PAA (10 mg/mL, pH 6.5) solution was added into 10 mL of bare MNP solution over 30 min. The solution was ultracentrifuged and the supernatant solution was decanted. The PAA-coated MNPs (0.5 bilayer) were then washed with 5 mL of water to remove any excess PAA. After that the 0.5 bilayer MNPs solution was redispersed into 10 mL water. One milliliter of 0.5 bilayer MNPs solution was taken out for UV–visible measurement. To keep the uniformity of the layer coating, 3.6 mL of PEI (10 mg/mL, pH 7.5) solution was added into the remaining 9 mL of 0.5 bilayer MNPs solution. The same steps were followed, and PAA/PEI-coated MNPs (one bilayer) were redispersed into 9 mL water. One milliliter of one bilayer MNP solution was also taken out for UV–visible measurement. To prepare a 1.5 bilayer sample, 3.2 mL of PAA solution was added into 8 mL of one bilayer MNPs solution. Through the same procedures, 1 mL of 1.5 bilayer MNPs solution was taken out for UV–visible test. Subsequently, 2.5, 3.5 and 4.5 bilayer samples were obtained for UV–visible measurement. The same volume of above-mentioned samples was added into 3 mL of ethanol to reduce the color of coated MNPs solution during UV–visible measurement.

2.4. Hydrogenation reactions

Catalytic hydrogenation was carried out in a 100 mL autoclave reactor containing 2 mL of MNPs coated with different bilayers of PAA/PEI–Pd(0) solution, substrate and a magnetic stir bar. The autoclave was flushed three times with H_2 gas and pressurized to 5 atm. All of the hydrogenation reactions were run at room temperature (25 °C). A high and constant rate of stirring was maintained throughout all hydrogenation reactions. Gas chromatography (YoungLin Acme 6000 m GC) was used to monitor the reactions. Turnover frequencies were calculated from the slopes of the linear portions of plots of percent hydrogenation versus time. Slopes were determined by forcing the intercept to be zero.

3. Results and discussion

3.1. Film deposition

In order to study the catalysis by nanoparticle-containing films, it is important to understand polyelectrolyte film growth and composition. UV–visible spectroscopy of MNP@PAA[PEI/PAA]$_n$ solutions in a quartz cell was performed to monitor the PAA/PEI multilayer fabrication on the surface of MNPs. As shown in Fig. 1, the intensity of the absorption band at 248 nm, attributed to the formation of PAA–PEI polyelectrolyte complex due to the charge attraction between PAA and PEI, increased linearly as the number of bilayers increased, indicating a stepwise and uniform assembly process. Therefore UV–visible spectra confirm the layer-by-layer growth of PAA/PEI films on the surface of MNPs.

The shape and size of MNP@PAA[PEI/PAA]$_5$ nanocomposite was directly determined by transmission electron microscopy

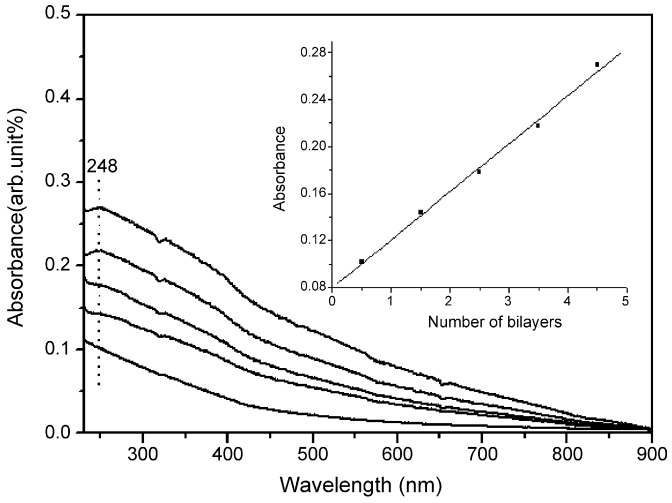

Fig. 1. UV–visible absorption spectra of MNP@PAA[PEI/PAA]$_n$ solutions. From lower to upper, the number of bilayers is 0.5, 1.5, 2.5, 3.5 and 4.5. Inset shows the absorbance at λ_{max} (248 nm) vs. the number of bilayers.

(TEM) (Fig. 2). It was clear that the organic polyelectrolyte polymers (lower contrast) were adsorbed onto the surface of MNP, and the average diameter of the core-shell nanocomposite of MNP and organic polymer was about 30 nm.

After Pd(II) solution reacted with PEI solution, UV–visible measurements of the product solutions were taken. As shown in Fig. 3, *t* the original absorption bands of PEI and Pd(II) disappeared; however one new absorption band at 292 nm was generated which was left shifted compared with the absorption band of Pd (II) at 319 nm. So we think that Pd ions in the PEI–Pd(II) solutions are actually bound to PEI. Considering the results shown Fig. 1 it was concluded that PAA/PEI–Pd(II) films also could be increased layer-by-layer on the surface of MNPs and held together by ionic cross-linking.

To further verify PAA/PEI–Pd(II) films growth on the surface of MNPs, the ICP-MS analysis of Pd was performed. Fig. 4 shows that the amounts of Pd in MNP@PAA[PEI–Pd(II)/PAA]$_n$

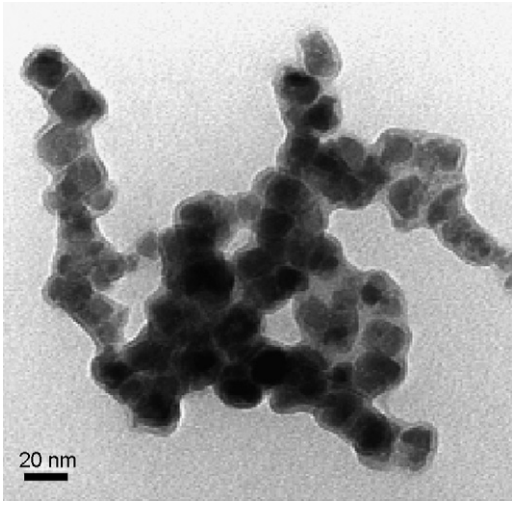

Fig. 2. TEM image of average 20 nm diameter MNPs coated with a total of 5.5 bilayers of PAA/PEI. The polyelectrolyte coating can be seen by TEM due to the different electron contrast of the core and coating.

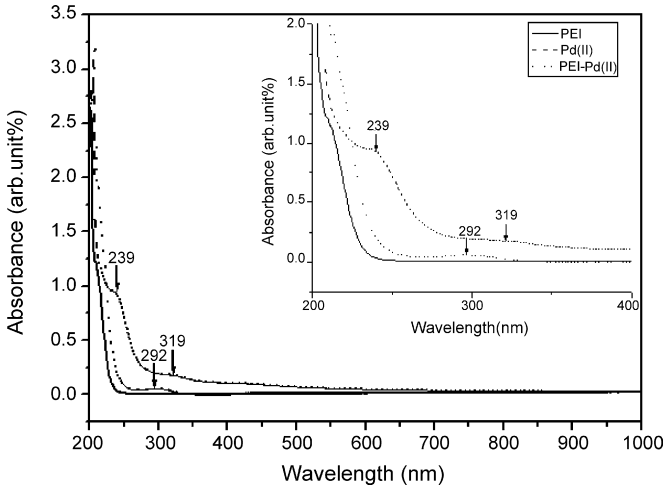

Fig. 3. UV–visible absorption spectra of PEI and PEI–Pd(II) solutions.

linearly increase as a function of the number of bilayers after deposition of the first layer. This data was consistent with the conclusion drawn from Figs. 1 and 3.

3.2. Film characterization

The formation of Pd nanoparticles by reduction with $NaBH_4$ in PAA/PEI–Pd(II) multilayer films was demonstrated by TEM observations. The sample was directly prepared on the carbon coated TEM Cu grid. The TEM image in Fig. 5 confirms the formation of Pd nanoparticles during exposure of PAA/PEI–Pd(II) films to $NaBH_4$ and the size of Pd nanoparticles ranging from 1 to 3 nm. They are homogeneously distributed throughout the whole film.

XPS provides information about the Pd oxidation state in reduced MNP@PAA[PEI–Pd(0)/PAA]$_n$ samples. Fig. 6 demonstrated the XPS spectra of MNP@PAA[PEI–Pd/PAA]$_3$ before and after reduction with $NaBH_4$. It showed that about 2/3 of the Pd(II) ions in the mutilayer polyelectrolyte films were reduced to Pd(0) after reduction with $NaBH_4$ probably due to the problem

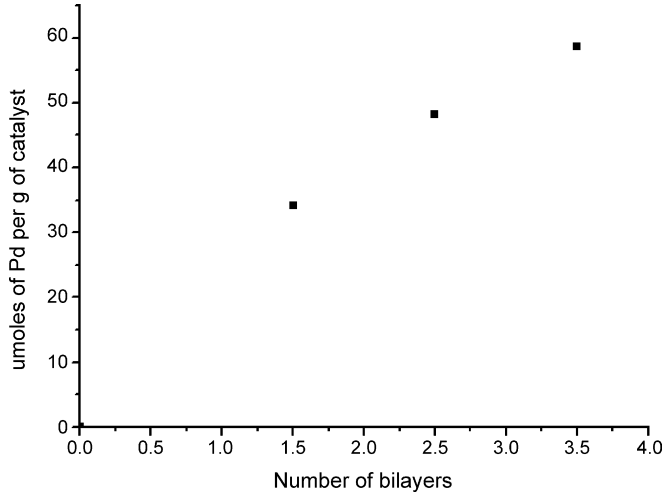

Fig. 4. Micromoles of Pd (determined by ICP-MS spectrometer)/g of catalyst for several values of *n* in reduced [PAA/PEI–Pd(0)]$_n$ films deposited on MNPs.

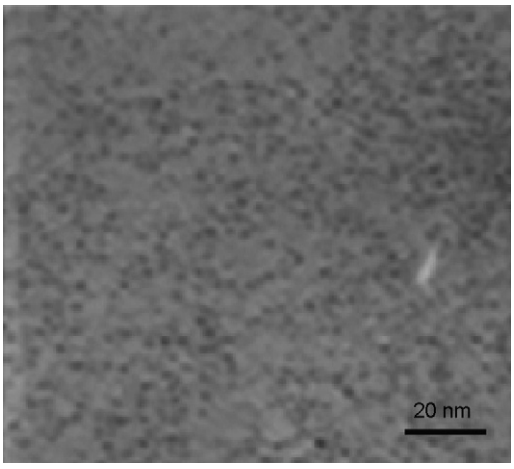

Fig. 5. TEM image of 3.5 bilayers of PAA/PEI–Pd(0) on a carbon coated copper grid.

of diffusion even in these thin multilayer films [30,31], generating new Pd(0) peaks at 335.38 ($3d_{5/2}$) and 340.59 ($3d_{3/2}$) eV, while the Pd $3d_{5/2}$ and $3d_{3/2}$ peaks corresponding to the Pd(II) ions with photoelectron energies of 340.44 and 345.6 eV were still detected, accounting for about 1/3 in intensity.

3.3. Catalysis of hydrogenation

A series of unsaturated alcohols was hydrogenated using the nanohybrid catalysts, MNP@PAA[PEI–Pd(0)/PAA]$_n$, to investigate the catalytic properties of reduced Pd in polyelectrolyte films. The hydrogenation rates were studied as a function of substrate concentration and film composition.

3.3.1. Reaction kinetics

Fig. 7 demonstrates how the rate of allyl alcohol hydrogenation catalyzed by reduced MNP@PAA[PEI–Pd(0)/PAA]$_1$ varies with the initial allyl alcohol concentration. As the concentration of allyl alcohols was increased, the conversion rate was also

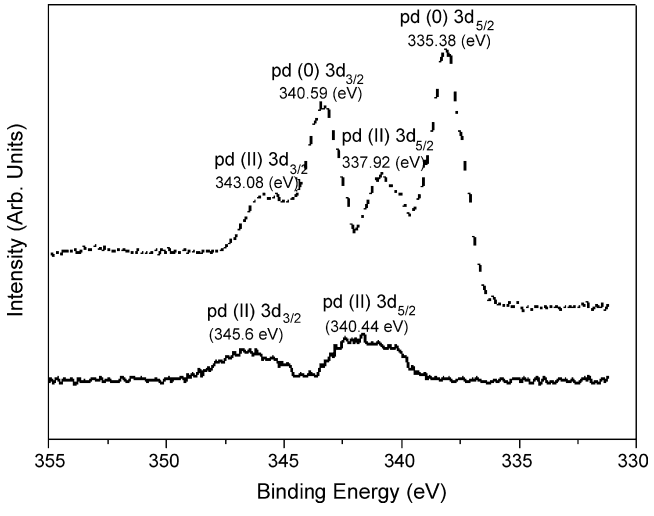

Fig. 6. XPS spectra of PAA[PEI–Pd/PAA]$_3$ film on MNPs before (bottom) and after (top) reduction with $NaBH_4$. The Pd $3d_{5/2}$ and $3d_{3/2}$ peaks are shown.

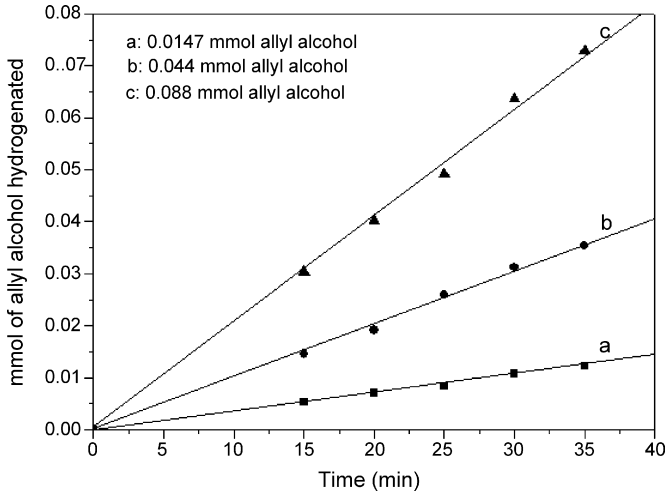

Fig. 7. Amount of allyl alcohol hydrogenated vs. reaction time: 5 mL solutions initially contain 4.76 mg of MNP@PAA[PEI–Pd(0)/PAA]$_1$ and various amounts of allyl alcohol (a) 0.0147 mmol, (b) 0.044 mmol and (c) 0.088 mmol.

increased by a factor of almost 1, implying that the hydrogenation reaction in our system is a first order reaction with respect to the substrates. It has been recently reported that the hydrogenation reaction, catalyzed by Pd nanoparticles embedded in polyelectrolyte multilayers, is a first-order reaction with respect to the initial concentration of alcohol, and that the reaction rates are consistent with diffusion-limited kinetics [32]. Therefore we can infer in our system the rate-limiting step of the reaction involves the diffusion of the substrate to the nanoparticles. Selectivities among substrates discussed below indicate that diffusion may be the rate-limiting process in the reactions.

3.3.2. Catalytic activity of reduced MNP@PAA[PEI–Pd(0)/PAA]$_n$ as a function of the substrate and film composition

Table 1 summarizes the turnover frequencies (TOFs) for the hydrogenation of several olefinic alcohols such as allyl alcohol (1), 3-buten-2-ol (2), and 1-penten-3-ol (3), which have different substituents at the α-carbon of the double bond

Table 1
TOFs for the hydrogenation of various olefin alcohols with MNP@PAA[PEI–Pd(0)/PAA]$_n$ catalysts with different numbers of n

Substrate	TOF (turnover frequency)[a]			
	$n=1$[b]	$n=2$[b]	$n=3$[b]	$n=7$[c]
1 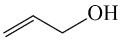	854/770	524/482	327/301	60
2 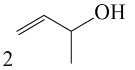	328/296	202/185	126/116	9
3 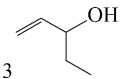	126/114	78/71	48/45	4

[a] mmol of hydrogenated olefin/mmol of Pd in hour.
[b] Two values are given to check the reproducibility of the same reaction with two different batches of each catalysts.
[c] For this hybrid composite catalyst, two bilayers of PAA/PEI–Pd(0) were capped with five bilayers of PAA/PEI having an actual structure of MNP@PAA[PEI–Pd(0)/PAA]$_2$[PEI/PAA]$_5$.

and generate different steric hindrances, in aqueous media and H_2 gas atmosphere. TOFs values of Pd nanoaprticles in MNP@PAA[PEI–Pd(0)/PAA]$_n$ hybrid composites decrease as the number of bilayers increases (columns 2–4 in Table 1), which reflects the almost constant reaction rate, although the actual amount of Pd in the hybrid composite is increased by about two and three times. This indicates that the hydrogenation reaction seems to be only catalyzed by Pd nanoparticles in the outermost layer of the hybrid composites, probably due to the restricted diffusion of olefinic alcohols into ionically cross-linked multilayer [PAA/PEI–Pd(0)]$_n$ films. Furthermore, a specially designed hybrid composite having five bilayers of PAA/PEI (containing no Pd) on two bilayers of PAA/PEI–Pd(0) was prepared and the TOFs values for the same olefinic alcohols were measured (column 5 in Table 1, $n=7$). By introducing the inactive additional layers, the hydrogenation reactivity was dramatically decreased by a factor of 8–20 depending on the olefinic alcohol structures (compare column 7 with column 2). The steric effect for the reactions (reactivity difference ratio of substrate 1 over substrate 3) was also increased from 8 to almost 15, resulting from a very slow diffusion of substrates through the LbL films of nanocomposites. This size-dependent reactivity in hydrogenation reaction implies that the polyelectrolyte LbL films restrict the access of the substrates to the active sites of Pd nanoparticles and size of substrates is the primary factor controlling the rate of hydrogenation.

3.3.3. *Recyclable of MNP@PAA[PEI–Pd(0)/PAA]$_n$ catalysts for hydrogenation reactions*

The hybrid composite catalysts, MNP@PAA[PEI–Pd(0)/PAA]$_n$, have a magnetic core and they can be isolated by applying an external magnetic field (using a commercial Nd–Fe-B magnet of ~0.3 T) and reused for consecutive reactions (Fig. 8). Before applying an external field, the magnetic nanocomposites were homogeneously dispersed to show their high catalytic activity (Fig. 8a). When the external magnetic field was applied after the reaction was completed, the magnetic nanocomposites were collected and the rest of the solution became clear within a couple of minutes (Fig. 8b). After the product solution was removed from the magnetic nanocomposites, a new batch of reagents was introduced and the mixture was vigorously stirred

Fig. 8. Images of the magnetic nanocomposites (a) without and (b) with an external magnetic field. The aggregations were formed when an external magnetic field was applied, which dispersed rapidly when the magnetic field was removed (within few minutes).

Table 2
Conversion yields of hydrogenation reaction with time (monitored by GC)

Time (h)	Conversion (%)
Substrate (allyl alcohol)	
0.5	72.3
1	78.9
2	82.9
3	84.9
4	90.9
5	89.1
19	88.9

Reaction conditions: 0.088 mmol of allyl alcohol with 4.76 mg of MNP@PAA[PEI–Pd(0)/PAA]$_1$ catalyst at 25 °C and 5 atm of H_2 for 4 h.

Table 3
Recycling experiments of the allyl alcohol hydrogenation reaction catalyzed by MNP@PAA[PEI–Pd(0)/PAA]$_1$[a]

Run	Yield[b] (%)
1	91.9
2	88.3
3	89.1
4	88.4
5	88.5
6	91.1
7	90.3
8	93.3
9	89.8
10	90.7

[a] Reaction conditions: 0.088 mmol of allyl alcohol with 4.76 mg catalyst at 25 °C and 5 atm H_2 for 4 h.
[b] Conversion yields were measured by GC.

to redisperse the aggregated magnetic nanocomposites rapidly into the reaction medium.

In order to check the recycling efficiency of the magnetic nanocomposite catalyst, the hydrogenation reaction of allyl alcohol (0.088 mmol) was investigated with MNP@PAA[PEI–Pd(0)/PAA]$_1$ (4.76 mg) catalyst. Preliminary checking reactions demonstrated that 4 h of reaction time was sufficient to achieve the yield of over 90% (Table 2). Even the reaction time extended to 19 h, the conversion of hydrogenation reaction still kept at about 90% without obvious decreasing. Under these reaction conditions, the hydrogenation of allyl alcohol was carried out 10 times with the recycled catalyst. As shown in Table 3, there was no significant change in the catalytic activity of the recycled magnetic nanocomposite even after being recycled 10 times (averaged 90.1%).

4. Conclusion

In conclusion, LbL depositions of PAA and PEI–Pd(II) onto the MNPs and the subsequent reduction of Pd (II) by $NaBH_4$ to Pd(0) provide a new method for synthesizing immobilized Pd nanoparticle catalysts. The polyelectrolyte matrix plays the role in stabilizing the nanoparticles and induces size selectivity of substrates. From the catalytic activity of these hybrid core-shell nanocomposites having different Pd structures in the hydrogenation of various olefin alcohols, it was concluded that only Pd

nanoparticles in the outermost layer of the hybrid composites worked as a catalyst, indicating that multilayer formation of Pd particles is not important for the catalytic application in LbL processes. Magnetic support makes the catalyst recycling from the reaction mixture so easy and simple that practical catalyst recycling is possible without showing any significant loss of catalytic activity. We expect this interesting property of hybrid composite catalyst systems to be applied to many other important industrial processes, and an investigation to set up more versatile methods is currently being carried out.

Acknowledgments

This work was supported by a grant from the National R&D Project for Nano Science and Technology of the KISTEP. The authors thank T.-J. Yoon and S.W. Ha for their valuable discussion and comments. Y. Wang is grateful for financial support from the BK21 program.

References

[1] R. Van Hardeveld, F. Hartog, Surf. Sci. 15 (1969) 189.
[2] J.P. Boitiaux, J. Cosyns, S. Vasudevan, Appl. Catal. 6 (1983) 41.
[3] C.E. Gigola, H.R. Aduriz, P. Bodnariuk, Appl. Catal. 27 (1986) 133.
[4] C.O. Bennet, M.J. Che, Catalysis 120 (1989) 293.
[5] J.S. Bradley, in: G. Schmid (Ed.), Clusters and Colloids: From Theory to Applications, VCH, Weinheim, 1994, p. 523.
[6] M.T. Reetz, R. Breinbauer, K. Wanninger, Tetrahedron Lett. 37 (1996) 4499.
[7] Y. Li, X.M. Hong, D.M. Collard, M.A. El-Sayed, Org. Lett. 2 (2000) 2385.
[8] J.H. Fendler, Nanoparticles and Nanostructured Films: Preparation, Characterization and Applications, Wiley–VCH, Weinhein, Germany, 1998.
[9] A. Benedetti, G. Fagherazzi, F. Pinna, G. Rampazzo, M. Selva, G. Strukul, Catal. Lett. 10 (1991) 215.
[10] R.L. Augustine, S.T. O'Leary, J. Mol. Catal. A: Chem. 95 (1995) 277.
[11] L. Piccolo, C.R. Henry, J. Mol. Catal. A: Chem. 167 (2001) 181.
[12] Y. Li, E. Boone, M.A. El-Sayed, Langmuir 18 (2002) 4921.
[13] T. Lopez, M. Asomoza, P. Bosch, E. Garcia-Figueroa, R. Gomez, J. Catal. 138 (1992) 463.
[14] K. Borszeky, T. Mallet, R. Eschiman, W.B. Schweizer, A. Baiker, J. Catal. 161 (1996) 451.
[15] S.D. Jackson, L.A. Shaw, Appl. Catal. A: Gen. 134 (1996) 91.
[16] B.M. Choudary, M.L. Kantam, N.M. Reddy, K.K. Rao, Y. Haritha, V. Bhaskar, F. Figueras, Appl. Catal. A: Gen. 181 (1999) 139.
[17] A. Korostylev, V. Tararov, C. Fischer, A. Monsees, A. Borner, J. Org. Chem. 69 (2004) 3220.
[18] J. Panpranot, L. Pattamakomsan, P. Praserthdam, J.G. Goodwin, Ind. Eng. Chem. Res. 43 (2004) 6014.
[19] J.P. Mathew, M. Srinivasan, Eur. Polym. J. 31 (1995) 835.
[20] H. Wellsted, E. Sitsen, A. Caragheorgheopol, V. Chechik, Anal. Chem. 76 (2004) 2010.
[21] M.O. Oyewumi, S. Liu, J.A. Moscow, R.J. Mumper, Bioconjugate Chem. 14 (2003) 404.
[22] S. Kidambi, J. Dai, J. Li, M.L. Bruening, J. Am. Chem. Soc. 126 (2004) 2658.
[23] S. Talae, Y. Akiyama, H. Otsuka, T. Nakamura, Y. Nagasaki, K. Kataoka, Biomacromolecules 6 (2005) 818.
[24] F. Caruso, H. Lichtenfeld, E. Donath, H. Mˆhwald, Macromolecules 32 (1999) 2317.
[25] F. Caruso, C. Schuler, D.G. Kurth, Chem. Mater. 11 (1999) 3394.
[26] F. Caruso, Chem. Eur. J. 6 (2000) 413.
[27] F. Caruso, Adv. Mater. 13 (2001) 11.
[28] M.H. Sousa, F.A. Tourinho, J. Depeyrot, G.J. da Silva, M.C.F.L. Lara, J. Phys. Chem. B 105 (2001) 1168.
[29] F.A. Tourinho, J. Depeyrot, G.J. da Silva, M.C.F.L. Lara, Braz. J. Phys. 28 (1998) 413.
[30] G. Kumar, J.R. Blackburn, R.G. Albridge, W.E. Moddeman, M.M. Jones, Inorg. Chem. 11 (1972) 296.
[31] R.W.J. Scott, H. Ye, R.R. Henriquez, R.M. Crooks, Chem. Mater. 15 (2003) 3873.
[32] S. Kidambi, M.L. Bruening, Chem. Mater. 17 (2005) 301.